PAPER • OPEN ACCESS

Stimulated Raman backscattering from a laser wakefield accelerator

To cite this article: A E Hussein et al 2018 New J. Phys. **20** 073039

View the article online for updates and enhancements.

Related content

- Relativistic laser–plasma interactions
  Donald Umstadter

- Quasi-monoenergetic multi-GeV electron acceleration by optimizing the spatial and spectral phases of PW laser pulses
  Junghun Shin, Hyung Taek Kim, V B Pathak et al.

- Laser wakefield acceleration in Kr–He plasmas and its application to positron beam generation
  Quratul Ain, Nasr A M Hafz, Song Li et al.

New Journal of Physics

The open access journal at the forefront of physics

PAPER

OPEN ACCESS

Stimulated Raman backscattering from a laser wakefield accelerator

A E Hussein[1] , J Ludwig[2], K Behm[1], Y Horovitz[1,4], P-E Masson-Laborde[3], V Chvykov[1,5], A Maksimchuk[1], T Matsuoka[1,6], C McGuffey[1,7], V Yanovsky[1], W Rozmus[2] and K Krushelnick[1]

[1] Center for Ultrafast Optical Science, University of Michigan, Ann Arbor, MI, 48109, United States of America
[2] Department of Physics, University of Alberta, Edmonton, Alberta, T6G 2J1, Canada
[3] CEA, DAM, DIF, F-91297, Arpajon, France
[4] Present address: Dynamical Experiments Group, Propulsion Division, Soreq NRC, Yavnee 81800, Israel.
[5] Present address: ELI-HU H-6720 Szeged, Dugonics tér 13, Hungary.
[6] Present address: Open and Transdisciplinary Research Initiative, OTRI, Osaka University, 2-1 Yamadaoka, Suita, Osaka, Japan, 565-0871.
[7] Present address: University of California San Diego, La Jolla, CA, 92093, United States of America.

E-mail: aehuss@umich.edu

Abstract

Experiments were performed using the HERCULES laser system at the University of Michigan to study backward stimulated Raman scattering (BSRS) from a laser wakefield accelerator driven with a 30 fs pulse. 'The spectrum of backscattered light was found to be significantly broadened and red-shifted in cases where electrons were accelerated. BSRS broadening (red-shifting) was found to increase with respect to both plasma density and accelerated electron charge for laser powers exceeding 100 TW. Two-dimensional Particle-in-Cell simulations reveal temporal dynamics for the BSRS emission, which ceases as the wakefield bubble is evacuated of plasma electrons because of relativistic self-focusing. The intensity and duration of the BSRS signal was found to vary with plasma density and laser intensity. Both experimental and simulation results indicate that backward SRS is associated with plasma electron density within the wakefield bubble. This measurement can serve as a diagnostic of bubble dynamics, and is correlated with trapped electron charge in this regime.

1. Introduction

Compact laser wakefield accelerators (LWFA) are part of a new generation of laser and plasma based accelerators, and are capable of generating GeV electron beams over a few centimeters (Tajima and Dawson 1979, Faure *et al* 2004, Geddes *et al* 2004, Mangles *et al* 2004, Leemans *et al* 2006, Esarey *et al* 2009, Wang *et al* 2013). Plasma wiggler radiation, generated by electron betatron oscillations in wakefield accelerators, results in spatially coherent x-rays having a brightness similar to that achievable with conventional accelerator technology, however with pulses on an unprecedented femtosecond timescale (Rousse *et al* 2004, Kneip *et al* 2010).

A LWFA is generated through the interaction of an intense, femtosecond laser pulse with a low density plasma. The ponderomotive force of the high-intensity pulse excites plasma waves in its wake that enable the trapping and acceleration of electrons to GeV energies from the longitudinal electric fields in the waves. LWFA at high power is associated with the formation of a nearly spherical bubble-shaped plasma wave that traps and accelerates electrons (Pukhov and Meyer-ter-Vehn 2002, McGuffey *et al* 2010, Palastro *et al* 2015). Although relativistic plasma waves are produced when the laser pulse duration is less than a plasma period, electron injection and acceleration only occurs when the driving pulse is at relativistic intensity (producing a very large amplitude wave).

Stimulated Raman Scattering (SRS) is a three-wave interaction that occurs in plasma at densities less than quarter critical ($n_c/4$), where the critical density is $n_c = m_e \omega_0^2 / 4\pi e^2$. Raman scattering involves the decay of the incident electromagnetic laser wave, ω_0, into an electrostatic plasma wave, ω_{pe}, and a scattered wave, $\omega_{scatt} = \omega_0 - \omega_{pe}$. For $n_e \ll n_c$, forward SRS results in the generation of relativistic plasma waves with wavelength $\lambda_p \simeq 2\pi c/\omega_{pe}$, while
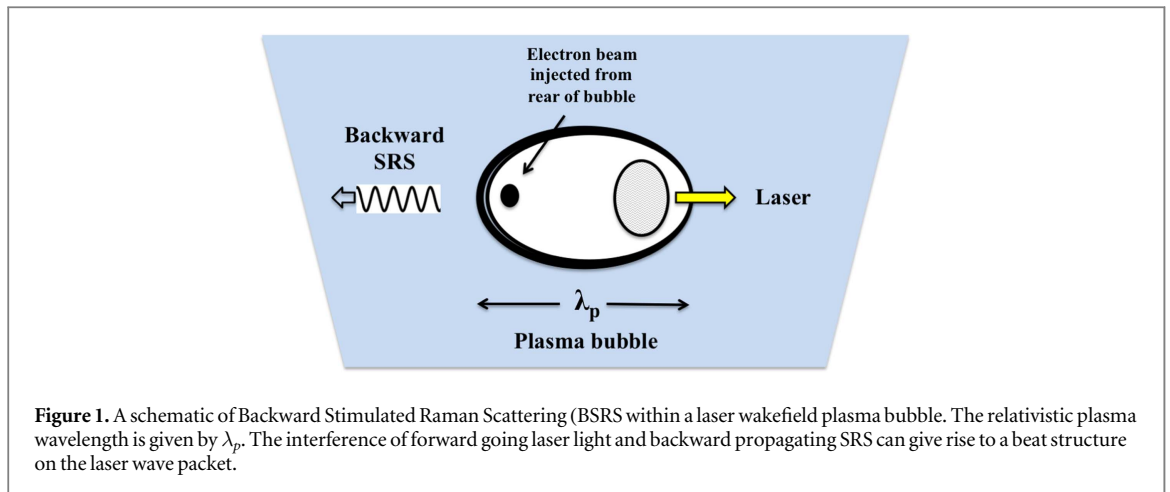
Figure 1. A schematic of Backward Stimulated Raman Scattering (BSRS within a laser wakefield plasma bubble. The relativistic plasma wavelength is given by λ_p. The interference of forward going laser light and backward propagating SRS can give rise to a beat structure on the laser wave packet.

backwards SRS generates non-relativistic waves with a wavelength $\lambda_p \simeq \lambda_0/2$. Interference between forward going light and backward propagating SRS light gives rise to a beat structure on a wave packet, which drives the plasma wave growth. A schematic of this interaction is given in figure 1. In the relativistic regime, where the electric field for electron acceleration is on the order of $m_e c^2/\lambda_p$, the laser pulse duration can be comparable to the growth rate of parametric instabilities such as SRS (Darrow *et al* 1992, Coverdale *et al* 1996, Ting *et al* 1996, Andreev and Kalmykov 1997, Miyamoto *et al* 1998).

For 'long' pulse durations (nanoseconds), Backward Stimulated Raman Scattering (BSRS) can lead to the scattering and redistribution of incident laser light as well as plasma heating and hot electron generation by SRS driven plasma waves. Therefore, the presence of BSRS for inertial confinement fusion-related studies has posed a challenge for effective laser–plasma coupling (Wilks *et al* 1995, Hinkel *et al* 2011). The spectral signatures of BSRS have been found to depend on laser intensity. At high intensities with picosecond duration pulses, spectra exhibit broadening and modulation of the frequency spectrum, potentially due to 'bursting' of the scattered light from the instability (rapid fluctuations in scattering intensity) (Darrow *et al* 1992, Krushelnick *et al* 1995, Coverdale *et al* 1996, Ting *et al* 1996, Miyamoto *et al* 1998). The spectra obtained from BSRS can be used as a diagnostic of the physics of high-intensity laser–plasma interactions (Krushelnick *et al* 1995, Ting *et al* 1996, Andreev and Kalmykov 1997, Jones *et al* 2002, Matsuoka *et al* 2010).

The duration of BSRS light is related to the propagation time of the laser pulse through the plasma, and therefore can be much longer than the incident laser pulse. Additionally, the growth rate of the SRS instability depends on the strength of the laser electric field, E, which is characterized by the dimensionless normalized vector potential, $a = v_{osc}/c = Ee/m_e\omega_0 c \propto I^{1/2}\lambda$, where v_{osc} is the peak quiver velocity, ω_0 and λ are the laser frequency and wavelength, respectively, and I is the laser intensity. For high-intensity laser pulses ($I > 10^{18}$ W cm^{-2}), the peak quiver velocity of an electron in the laser field can approach the speed of light, resulting in growth rates of the SRS instability that exceeds the electron plasma frequency $\omega_{pe} = (4\pi n_e^2/m_e)$. This is known as the *strongly coupled* regime, and is associated with frequency components shifted to multiples of the plasma frequency ω_{pe}, resulting in a highly broadened spectrum that is not clearly connected to the laser spectrum (Andreev and Kalmykov 1997).

Strongly coupled SRS measurements from picosecond duration ($\simeq 800$ fs) pulses have been previously made, with the width of the spectra exceeding the plasma frequency (Darrow *et al* 1992). A transition from classical to anomalous (broadened) BSRS with increasing laser intensity has been observed experimentally from 600 fs laser pulses (Coverdale *et al* 1996). Additionally, measurements from 450 fs high-intensity ($I > 10^{18}$ W cm^{-2}) laser pulses have yielded spectra with large amplitude modulations (Ting *et al* 1996). Experimental measurements of BSRS from 120 fs pulses at sub-relativistic intensities have also been reported, where the amount of backscattered light was found to decrease at low pressures due to the ponderomotive expulsion of electrons along the laser axis (Malka *et al* 1996). BSRS measurements have also been made during LWFA with laser powers up to 8 TW (max intensity of $\simeq 2 \times 10^{19}$ W cm^{-2}) (Kaganovich *et al* 2016). Kaganovich *et al* observed saturation of BSRS signal due to strong self-focusing at increasing gas pressures (plasma densities). Their experimental results were consistent with BSRS generation in the weakly nonlinear regime, where the growth rate of SRS is positive only in a very narrow spectral region, resulting in a frequency component of the laser pulse with a width less than ω_{pe}.

The observation of these broadened, highly modulated BSRS spectra, which are not predicted by the standard parametric theory of SRS, highlights the role of nonlinear dynamics in electron plasma wave (EPW) generation (Škorić *et al* 1996, 2013). For high-intensity, short-pulse interactions, very large amplitude EPWs are produced, in which the oscillating electrons can have very high velocities. To account for the relativistic

correction to electron mass (nonlinear detuning) at these intensities, Kono and Škorić included a nonlinear term in their one-dimensional model of SRS in a weakly collisional plasma (Kono and Škorić 2010). Their theory predicts a saturation of backscattered light for lower laser pump amplitudes, given by the ratio of the electron quiver velocity in a laser pump field to the speed of light ($eE_0/m_e\omega_0 c$), revealing quasiperiodic structures. However, with increasing pump strength, pronounced spectral broadening and chaotic bursting of backscattered emission was observed, indicating a transition to chaos and eventual loss of coherent modulation. 1D-PIC simulations of Raman backscattered spectra were found to produce modulated spectra with increasing complexity as a function of pump strength, agreeing with experimental measurements from a 0.8 ps laser pulse by Darrow *et al* (1992). Therefore, the extreme broadening of backscattered spectra may indicate scattering from many unstable plasma modes in the strongly coupled regime due to loss of coherence of plasma waves during wave breaking (Darrow *et al* 1992, Andreev and Kalmykov 1997, Walton *et al* 2006). Broadening may also be due to spatiotemporal localization (bursting) of the Raman scattered light within the laser pulse from a rapid saturation of the SRS instability (Walton *et al* 2006, Škorić *et al* 2013).
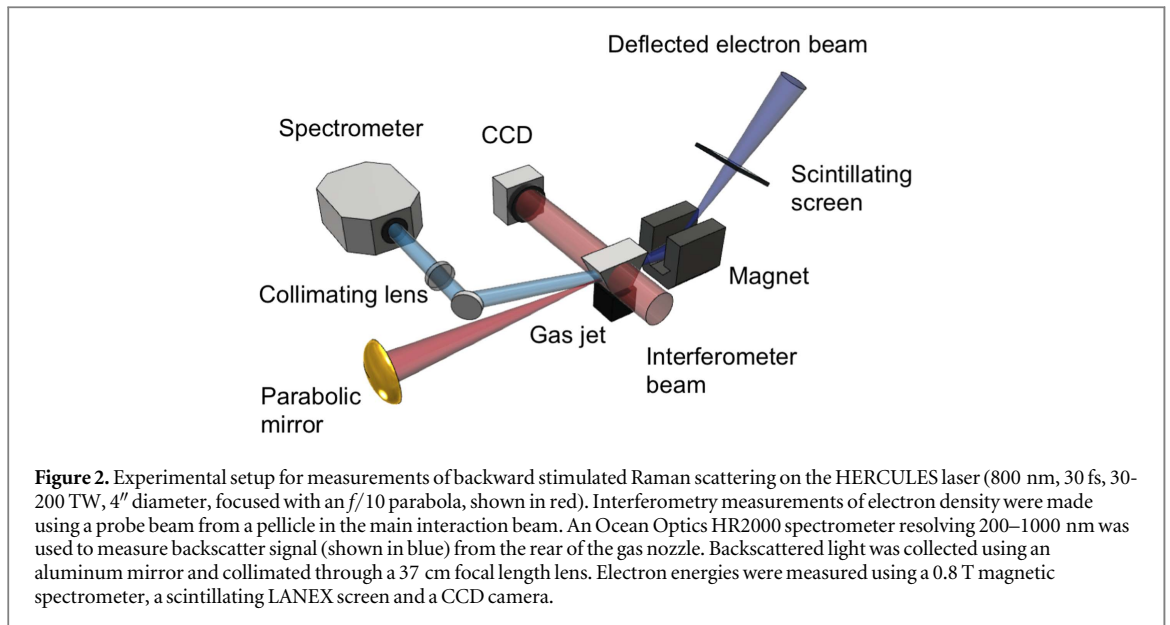
Additionally, electron injection and trapping during LWFA is connected with the wave breaking of EPWs having phase velocities approaching the speed of light (Walton *et al* 2006). Instabilities with a self-modulating laser pump can couple to relativistic plasma waves, creating new sidebands in the forward spectra, and contributing to the growth and ultimate breaking of these EPWs (Andreev and Kalmykov 1997, Walton *et al* 2006). However, severe side scattered SRS has been found to degrade electron beam quality in LWFA through the seeding of filamentation instabilities in the electron beam, as well as erosion of the incident laser pulse (Matsuoka *et al* 2010).

Backward SRS in the strongly coupled (strongly nonlinear) regime during LWFA has not previously been observed experimentally. In the bubble regime of LWFA, the importance of this phenomenon is also unclear, however the backward SRS may generate large amplitude short wavelength plasma waves in a partially 'evacuated' plasma bubble, which may affect the dynamics of electron injection and acceleration in this regime. Previous studies motivate measurements of backscattered spectra produced at these ultra-short-pulse durations as a diagnostic of the interaction. Of particular interest is the efficiency and control of electron self-injection, which may potentially enable optimization of the LFWA mechanism, and generation of electron beams with higher charge. The utilization of BSRS to generate a counter-propagating photon beam could also be used to produce x-rays by the Compton scattering of photons with energetic electrons accelerated by LWFA (Palastro *et al* 2015, Kaganovich *et al* 2016). This method of all-optical Compton scattering could produce x-rays with a wide range of energies up to 1MeV, and could provide a compact alternative to existing linear electron accelerator devices. Photons generated via BSRS may provide a more tractable realization of all-optical Compton scattering as compared to the use of two separate ultra-short pulses to generate the energetic electron–photon interaction.

In this paper, we describe experiments conducted using the HERCULES laser system at the University of Michigan to measure backward SRS generated during LWFA in the strongly coupled regime. Resultant backscatter spectra were found to be highly modulated and significantly red-shifted in cases where electrons were accelerated. A correlation between the total amount of BSRS and charge of the accelerated electron beam was observed for laser powers exceeding 100 TW. The amount of BSRS (characterized by the intensity of the of the measured spectrum beyond 830 nm) was also found to increase as a function of plasma density at these powers. For laser powers above 100 TW, where the ponderomotive force of the laser is higher, the BSRS signal was significantly less red-shifted, while still correlating with electron beam charge and plasma density. For laser powers below 50 TW, no such correlations were observed. Therefore, it is clear that the red-shift broadening of the backward SRS spectrum is associated with increased electron beam charge in a LWFA. These experiments were complemented by two-dimensional PIC simulations that indicate growth of BSRS until the wakefield bubble is evacuated of electrons due to relativistic self-focusing of the laser. Simulations and experiments indicate that measurement of backward propagating SRS may be used as a diagnostic of bubble formation and trapped electron charge within the bubble. A summary of the experimental setup is given in section 2, PIC simulations are described in section 3, and results and analysis are given in section 4.

2. Experimental setup

At the University of Michigan, experiments were conducted using pulses from the HERCULES Ti:sapphire laser system. The laser operates at a wavelength of 800 nm with 30 fs pulse duration. Pulses with powers between 20 and 180 TW (1.3×10^{19} W cm^{-2}–1.1×10^{20} W cm^{-2}) were focused using an $f/10$ off-axis parabolic mirror onto a pulsed gas jets generated from gas jet nozzles between 1.55 and 5 mm in diameter. A deformable mirror was used to correct the laser wave front and produces a focal spot with a full-width-half-maximum of 10 μm.

Figure 2. Experimental setup for measurements of backward stimulated Raman scattering on the HERCULES laser (800 nm, 30 fs, 30-200 TW, 4″ diameter, focused with an *f*/10 parabola, shown in red). Interferometry measurements of electron density were made using a probe beam from a pellicle in the main interaction beam. An Ocean Optics HR2000 spectrometer resolving 200–1000 nm was used to measure backscatter signal (shown in blue) from the rear of the gas nozzle. Backscattered light was collected using an aluminum mirror and collimated through a 37 cm focal length lens. Electron energies were measured using a 0.8 T magnetic spectrometer, a scintillating LANEX screen and a CCD camera.

Gas jet pressures up to 800 psi of helium gas were utilized, yielding plasma densities up to 6×10^{19} cm^{-3}. Backscattered light was collected using an aluminum mirror at an angle of 5.5° from the nozzle and collimated onto the entrance slit of an Ocean Optics HR2000 spectrometer (200–1100 nm). The laser spectral bandwidth was measured to be 30 nm; therefore, for backscattering measurements the area under the red-shifted spectrum was considered for wavelengths beyond 830 nm. The region was chosen to avoid errors due to scattered light inside the target chamber, and is taken as a Figure-of-Merit of the total BSRS signal due to the approximate symmetry of the spectrum. An electron spectrometer (using a 0.8 T magnet) with a LANEX phosphor scintillating screen and a charge coupled device camera enabled electron energy detection between 47 and 800 MeV. Interferometer measurements of the plasma density were obtained using a transverse probe beam. A schematic of the setup is given in figure 2.

3. Particle-in-Cell (PIC) simulation parameters

Two-dimensional simulations of a 30 fs, 800 nm laser pulse at 100 and 140 TW in varying plasma densities were performed using the relativistic PIC code SCPIC (Popov *et al* 2010), which has previously been used to study electron acceleration in the bubble regime (Masson-Laborde *et al* 2014). These simulations provide additional insight on the kinetic processes leading to SRS and particle loading. Simulations used a domain of $400 \, \mu$m $\times$ 200 μm with resolution 12000 $\times$ 6000 cells (30/μm) and 16 particles per cell. Electron plasma densities of $(0.5–2) \times 10^{19}$ cm^{-3} were simulated, assuming a plasma temperature of 50 eV. Several diagnostic probes were placed on the simulation boundaries to record SRS as the laser propagated in the *x*-direction through the plasma. A linear density ramp of 100 μm from vacuum to full density was included in the model.

4. Results and analysis

A typical experimental BSRS spectrum obtained from 30 fs laser pulses at 50 and 180 TW is given in figure 3(a). A background backscatter shot without gas is also plotted for comparison. Dramatic broadening and modulation of the BSRS spectrum is observed at all powers with the generation of an electron beam. The laser intensity is centered at 800 nm and a red-shift in the BSRS spectrum was considered as signal extending beyond 830 nm (with 30 nm taken as the nominal spread of the laser wavelength). The integrated area under the red-shifted BSRS spectrum is taken as a Figure-of-Merit of the total BSRS signal, since the measured spectrum is approximately symmetric.

The spectrum measured without gas in figure 3(a) resembles the laser spectrum and results from stray light scattering inside the target chamber. We note here that the signal level within the incident laser spectrum is negligibly weaker than the shots with gas and the BSRS signal dominates the signal. The observed broadening and modulation of the BSRS spectrum are similar to measurements at longer pulse durations in the strongly coupled regime (Darrow *et al* 1992, Coverdale *et al* 1996). However, the modulation of the spectrum is more pronounced than any previously observed.
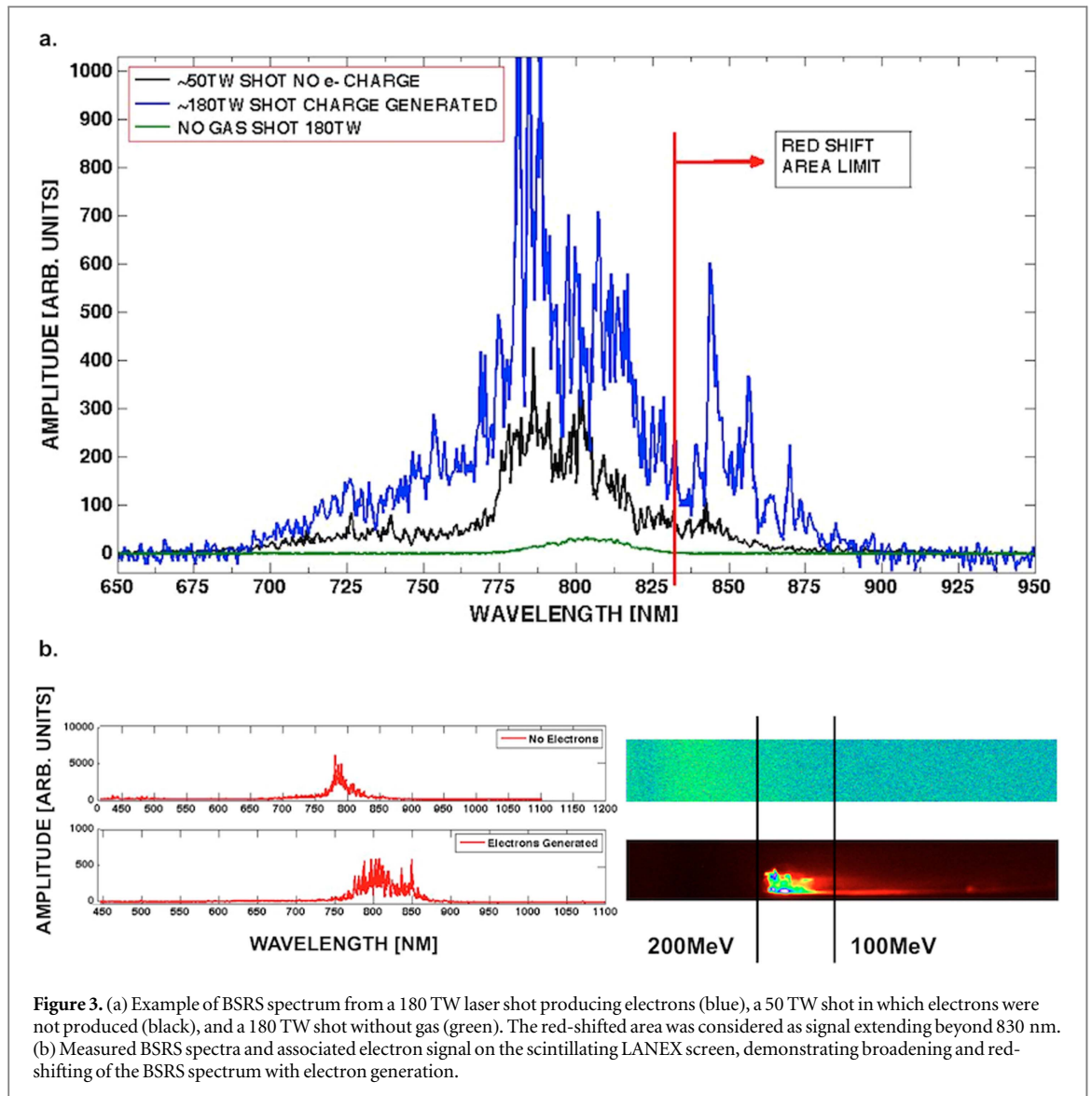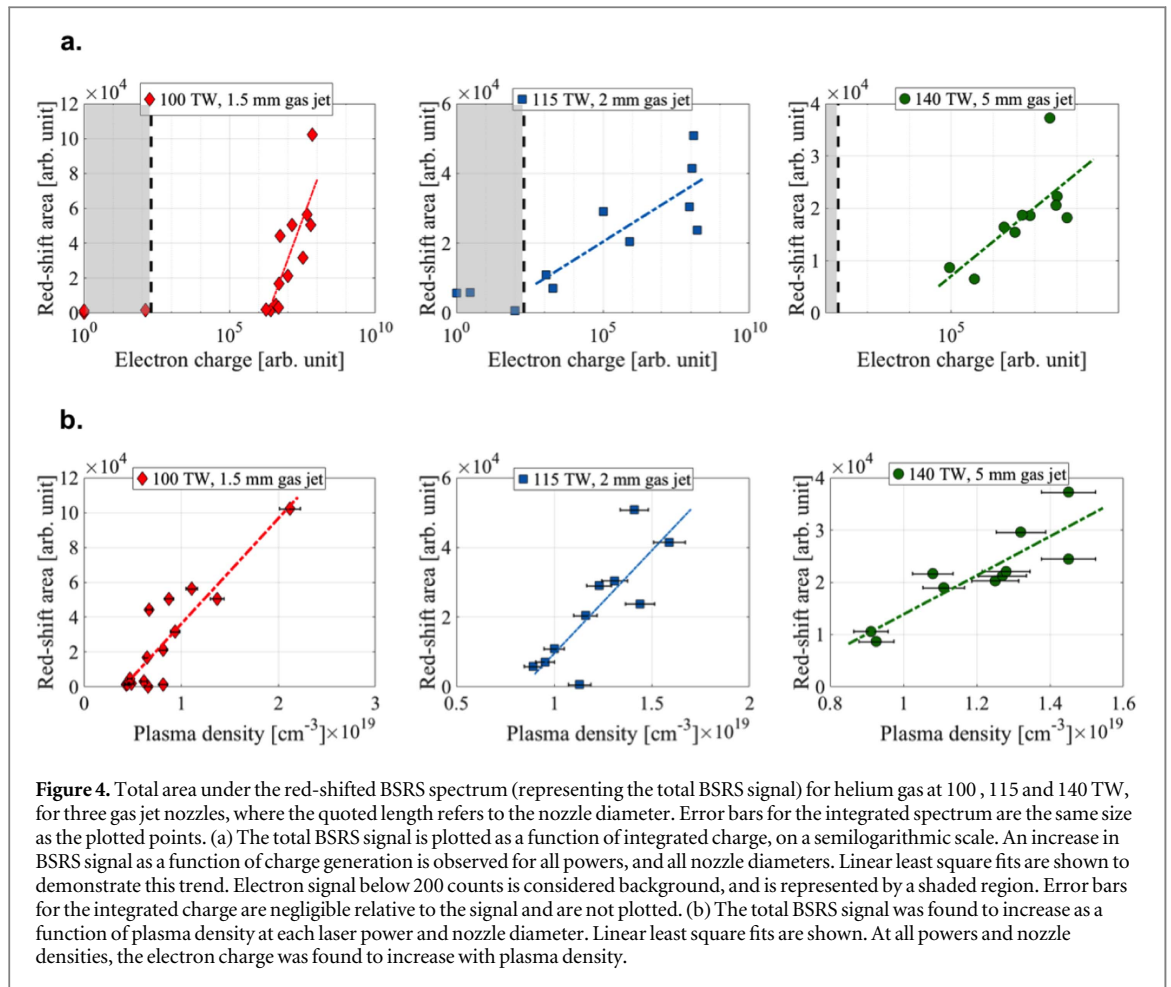
Figure 3. (a) Example of BSRS spectrum from a 180 TW laser shot producing electrons (blue), a 50 TW shot in which electrons were not produced (black), and a 180 TW shot without gas (green). The red-shifted area was considered as signal extending beyond 830 nm. (b) Measured BSRS spectra and associated electron signal on the scintillating LANEX screen, demonstrating broadening and red-shifting of the BSRS spectrum with electron generation.

A comparison between BSRS spectrum with and without electron generation is given in figure 3(b) with associated electron signal. These measurements were obtained at a laser power of 30 TW, using a 1.5 mm diameter gas jet nozzle. No specific correlations between the energy spread of the electron beams and the amount of SRS were observed. Electron measurements shown in this figure correspond to signal from the magnetic spectrometer on a scintillating LANEX screen. The contrast on each LANEX image is optimized to show variation in the signal above background, therefore these images do not have the same contrast.

BSRS broadening was found to increase with electron beam charge generation and plasma density for laser powers at and above 100 TW. Measurements taken at 100 TW, 115 TW and 140 TW, with 1.5 mm, 2 mm and 5 mm diameter gas jet nozzles, respectively, are presented in figure 4. The integrated signal in the red-shifted BSRS spectrum as a function of electron charge is plotted on a semilogarithmic scale in figure 4(a), and as a function of plasma density in figure 4(b). Plasma density was determined from interferometry images. Electron charge, presented in arbitrary units, refers to the integrated electron signal from the magnetic spectrometer on the scintillating screen. All signal below 200 counts is considered background, and for all shots with near-zero BSRS there was also near-zero electron charge. For each power and nozzle diameter, each plotted point corresponds to a single laser shot from a single experimental run. The plotted data reflects all points obtained under the same experimental conditions (quoted power and nozzle diameter).

Linear least squares fits are plotted for each power to highlight an increase in BSRS as a function of electron charge on a semilogarithmic scale in figure 4(a), and an increase in BSRS as a function of plasma density on a linear scale in figure 4(b). However, these fits should not be considered as a scaling, as the process is highly nonlinear. Note that the y-axis varies for each plot, with the total BSRS signal decreasing with increasing power. The total BSRS signal is greatest at 100 TW. Additionally, at laser powers at and above 100 TW, the integrated

Figure 4. Total area under the red-shifted BSRS spectrum (representing the total BSRS signal) for helium gas at 100 , 115 and 140 TW, for three gas jet nozzles, where the quoted length refers to the nozzle diameter. Error bars for the integrated spectrum are the same size as the plotted points. (a) The total BSRS signal is plotted as a function of integrated charge, on a semilogarithmic scale. An increase in BSRS signal as a function of charge generation is observed for all powers, and all nozzle diameters. Linear least square fits are shown to demonstrate this trend. Electron signal below 200 counts is considered background, and is represented by a shaded region. Error bars for the integrated charge are negligible relative to the signal and are not plotted. (b) The total BSRS signal was found to increase as a function of plasma density at each laser power and nozzle diameter. Linear least square fits are shown. At all powers and nozzle densities, the electron charge was found to increase with plasma density.
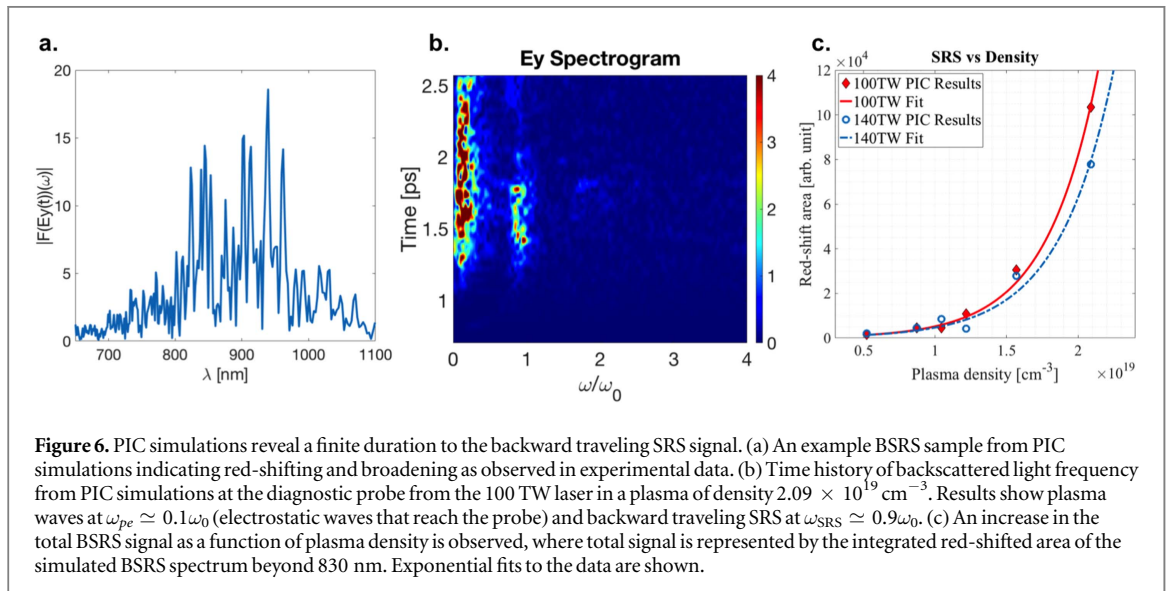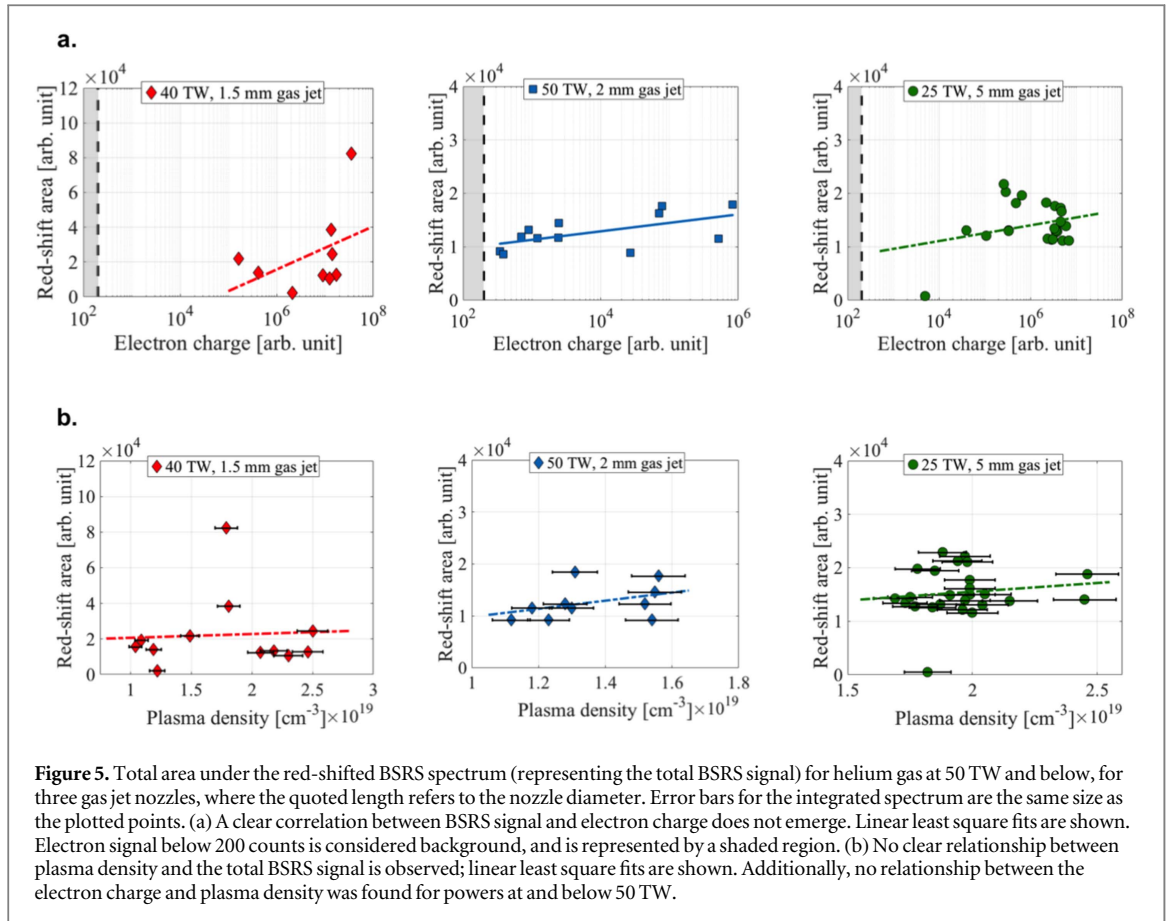
electron charge was found to increase with increasing plasma density. Correlations between BSRS signal and electron and plasma density are persistent for all nozzle diameters.

For powers of 50 TW and below, variations in the BSRS signal with electron charge are not as dramatic. This is shown in figure 5(a). For helium gas targets at powers from 25 to 50 TW a clear trend is not obvious across all powers and nozzle diameters. Linear least squares fits to the semilogarithmic plot as a function of electron charge are shown for comparison with figure 4(a); the total red-shifted area (and therefore the total BSRS), does not appear to increase with the total charge in the resultant electron beam. Additionally, at these lower powers, no clear correlation between the total BSRS signal and plasma density is observed. This data is plotted in figure 5(b). Linear least squares fits are also shown for comparison with the high power trends in figure 4(b). No obvious trend between BSRS signal and plasma length can be observed.

The results in figures 4 and 5 indicate that the intensity and broadening of the BSRS spectrum is most pronounced at powers above 100 TW. Additionally, the total area under the BSRS spectrum at powers below 100 TW was nearly half that observed for higher laser powers. The increased bandwidth and 'spikey' structure of BSRS spectrum may indicate very rapid growth rate and saturation of the backward SRS instability at high laser powers.

Two-dimensional PIC simulations enabled a detailed analysis of BSRS production in a LWFA. Backward SRS signal was observed in the SCPIC simulations and the time history was recorded. Typical probe spectra are shown in figures 6(a) and (b). Numerical simulations also reproduce the highly modulated experimental backscatter spectrum, indicating the applicability of PIC simulations for modeling SRS in LWFA interactions. The production of anomalous spectra may also may also be influenced by relativistic frequency shifts in plasma waves, as predicted in calculations by Škorić *et al* (2013), wherein pronounced anomalous spectra, characterized by broadening and chaotic bursting, indicated a loss of coherent modulation for high laser intensities. However, no relativistic plasma waves due to BSRS, as postulated by Škorić *et al* (2013), were observed.

The BSRS spectrum was recorded from PIC simulation probes for laser powers of 100 and 140 TW. The integrated area under the red-shifted spectrum (beyond 830 nm), representing the total BSRS signal, is plotted as a function of plasma density in figure 6(c). Each point corresponds to a single laser event. An increase in the total BSRS signal as a function of plasma density is observed and exponential fits to the data are shown. As in the

Figure 5. Total area under the red-shifted BSRS spectrum (representing the total BSRS signal) for helium gas at 50 TW and below, for three gas jet nozzles, where the quoted length refers to the nozzle diameter. Error bars for the integrated spectrum are the same size as the plotted points. (a) A clear correlation between BSRS signal and electron charge does not emerge. Linear least square fits are shown. Electron signal below 200 counts is considered background, and is represented by a shaded region. (b) No clear relationship between plasma density and the total BSRS signal is observed; linear least square fits are shown. Additionally, no relationship between the electron charge and plasma density was found for powers at and below 50 TW.

Figure 6. PIC simulations reveal a finite duration to the backward traveling SRS signal. (a) An example BSRS sample from PIC simulations indicating red-shifting and broadening as observed in experimental data. (b) Time history of backscattered light frequency from PIC simulations at the diagnostic probe from the 100 TW laser in a plasma of density $2.09 \times 10^{19} \, \mathrm{cm^{-3}}$. Results show plasma waves at $\omega_{pe} \simeq 0.1\omega_0$ (electrostatic waves that reach the probe) and backward traveling SRS at $\omega_{SRS} \simeq 0.9\omega_0$. (c) An increase in the total BSRS signal as a function of plasma density is observed, where total signal is represented by the integrated red-shifted area of the simulated BSRS spectrum beyond 830 nm. Exponential fits to the data are shown.

experiments, PIC simulations show an increase in the SRS signal with plasma density and confirm that the 100 TW laser pulse typically produces more SRS than the 140 TW laser pulse.

PIC simulation results also reveal a finite duration to the BSRS signal, as shown in the backscatter diagnostic probe of figure 6(b). While bubble formation begins almost immediately upon the laser entering the plasma, the bubble is not completely evacuated of electrons until the laser is self-focused to sufficiently high-intensity. During the period when there is finite electron plasma density inside the bubble, BSRS is produced from the laser, and once the bubble is evacuated the scattering stops.

A significant BSRS signal is observed only in simulations where the laser intensity is below the critical intensity for complete blowout of electron density in a bubble (Lu *et al* 2006). For 100 TW laser power, complete blowout occurs at plasma densities below $1.2 \times 10^{19} \, \mathrm{cm^{-3}}$ (see figure 6(c)). At higher densities, the balance

Figure 7. 2D PIC simulations of the 100 TW laser in a plasma of density 1.56×10^{19} cm^{-3}. (a) Plasma electron density at $t = 0.75$ ps, showing finite electron density inside the LWFA bubble resulting in SRS. (b) Plasma electron density at $t = 1.00$ ps, showing complete evacuation of electrons from the LWFA bubble due to relativistic self-focusing of the laser. (c) Laser amplitude and plasma density versus propagation distance 1D cut along x, at $y = L_y/2 = 100\,\mu$m at $t = 0.75$ ps and (d) $t = 1.00$ ps.

between the ponderomotive force of the laser and the force that arises due to the charge separation may allow for finite electron density inside the bubble.

For all the sub-critical laser intensity simulations, the evacuation of the wakefield bubble and termination of backward SRS occurred at about 700 fs after the laser entered the plasma. Figure 7 shows 2D simulations and line-outs of plasma electron density as a function of time, indicating complete evacuation of electrons due to relativistic self-focusing of the laser after a propagation time of about 1 ps (simulation time).

By using the theory for complete electron blowout given by Lu *et al* (2006), Esarey *et al* (2009), one can estimate the amplitude of the laser pulse required for complete evacuation of the bubble for a given plasma density. Laser pulses with initial electric field amplitude below this threshold will first undergo relativistic self-focusing before complete evacuation of the bubble occurs.

Combining the laser amplitude requirements with a theory for relativistic self-focusing (Sprangle *et al* 1990, 1992) results in a critical length parameter that determines the distance the laser pulse must travel in the plasma before its bubble is completely evacuated:

$$z_c = Z_R \sqrt{\left[\frac{a_0}{a_c} - 1\right]\left(1 - \frac{P}{P_c}\right)^{-1}}, \tag{1}$$

$$a_c = \left[\frac{b^2}{2} + \frac{1}{2}(b^4 + 4b^2)^{1/2}\right]^{-1/2}, \tag{2}$$

$$b = ((k_p r_0)/2)^2, \tag{3}$$

where the real component of z_c is defined to be the critical length for blowout (i.e. restricting $a_0 \leqslant a_c$ and $P > P_c$), Z_R is the laser Rayleigh length, a_0 is the initial normalized amplitude of the laser, a_c is the critical laser amplitude for complete blowout (Lu *et al* 2006, Esarey *et al* 2009), P/P_c is the ratio of the laser power to the critical power for relativistic self-focusing, $k_p = \omega_{pe}/c$ is the plasma wavenumber, and r_0 is the diffraction limited spot size of the laser.

The amplitude threshold for the blowout increases with density, and the critical power P_c for the relativistic self-focusing decreases with higher plasma densities. This results in a nearly constant critical length z_c (independent of plasma density) for lasers with initial amplitude below the threshold for complete bubble evacuation. The critical length (1) $z_c \approx 33\ \mu$m for 100 TW lasers, corresponding to $n_e > 1.2 \times 10^{19}\ \mathrm{cm}^{-3}$. To estimate z_c from the simulation results, see figures 7(c), (d), one could evaluate the distance between the beginning of the homogeneous plasma at the end of the density ramp, $x \approx 200\ \mu$m in figure 7(c), and the location of the fully evacuated electron density in figure 7(d) at $x \approx 270\ \mu$m. The extent of the critical length, $z_c \approx 70\ \mu$m, observed in PIC simulations corresponds very well to the region of the strong BSRS signal and corresponding duration of the scattered signal at the probe (see figure 6(b) and note that due to the counter propagation of the laser and its SRS, the duration of the scattered light signal is expected to be $2z_c/c$). Also, $z_c \approx 70\ \mu$m remains nearly constant in all runs at different plasma densities. The observed discrepancy between theoretical prediction and PIC results are well within the expected limitation of the scaling argument in equation (1) and rough estimates based on the simulation results in figure 7.

While finite densities in the bubble (due to sub-critical laser amplitudes for the full electron evacuation) result in the strongest BSRS signals in the short PIC simulations, there is always SRS present due to plasma density at the front of the bubble (see figure 7(d)), which is also lower for higher intensity lasers because of the steeper density gradient. This BSRS produced at the front of the bubble is less prominent in the short PIC simulations.

PIC simulations indicate that BSRS signal persists until the wakefield bubble is evacuated due to relativistic self-focusing of the laser. Thus, measurement of backward propagating SRS appears to be a result of non-zero electron plasma density within the bubble. One explanation for this correlation is that the BSRS instability may be seeded by noise produced by electron injection into the bubble during self-focusing. Consequently, BSRS signal and time-resolved backscattered spectra may be useful as a diagnostic of bubble formation and trapped electron charge.

5. Conclusions

In this paper, we present the first experimental measurements of backward strongly coupled SRS in the bubble regime of LWFA. The observed spectra are unlike those observed in previous experiments, and are characterized by a very spikey structure, consistent with 2D PIC simulations, see figure 6(a). The observed backward Raman spectrum is correlated with enhanced electron charge in the accelerated beam. For laser powers at and above 100 TW, the integrated BSRS spectrum at wavelengths beyond 830 nm (representing the total BSRS signal) was found to increase with both electron charge and plasma density. For laser powers below 100 TW, no such correlation was observed.

Two-dimensional PIC simulations show a correlation between BSRS signal and plasma electron density within the laser wakefield bubble. For increasing laser intensities, the intensity and duration of the BSRS signal decreases as electron density within the bubble is rapidly depleted. The BSRS signal is enhanced when the electron density in the bubble is non-zero. The broadened, highly modulated spectra obtained from backscattered light are also observed in PIC simulations. They are results of rapid variations in the background plasma conditions during bubble formation and scattering of backscattered light on the secondary plasma wakes that are formed behind the primary bubble containing the short laser pulse. It has has been shown in the past that wake formation contributes to the frequency shifts of the laser pulse (Shadwick *et al* 2009, Ludwig *et al* 2018), and this in turn affects spectrum of the scattered light. These spectra of scattered light are reminiscent of the transition to chaos and eventual loss of coherence due to nonlinear detuning at relativistic laser intensities (Kono and Škorić 2010, Škorić *et al* 2013). However, no such transition has been observed in PIC simulations with varying laser powers. In addition, the low BSRS reflectivity would not be sufficient to produce relativistic Langmuir waves that would be responsible for such frequency shifts.

These results indicate that at highest powers (100 TW and above), the bursting, broadening and modulation of the BSRS frequency spectrum is associated with increased plasma density within the LWFA plasma bubble. The existence of a non-evacuated wakefield bubble, as indicated by backward SRS signal, may be related to enhanced electron injection, resulting in enhanced charge in the accelerated electron beam. The correlation observed between electron beam charge and BSRS is likely due to density fluctuations in the plasma, which may be due to the injection of electrons into a LWFA bubble. These fluctuations can provide a seed for the development of the BSRS instability. Therefore, it is possible that fluctuations due to BSRS can provide feedback for electron injection.

Acknowledgments

ORCID iDs

A E Hussein ● https://orcid.org/0000-0001-9676-4862
K Krushelnick ● https://orcid.org/0000-0001-9116-9511

References

Andreev N and Kalmykov S Y 1997 *Phys. Lett.* A **227** 110–6

Coverdale C, Darrow C, Decker C, Naumova N, Esirkepov T Z, Sakharov A, Bulanov S, Mori W and Tzeng K 1996 *Plasma Phys. Rep.* **22** 617

Darrow C B, Coverdale C, Perry M D, Mori W B, Layton C, Marsh K and Joshi C 1992 *Phys. Rev. Lett.* **69** 442

Esarey E, Schroeder C B and Leemans W P 2009 *Rev. Mod. Phys.* **81** 1229

Faure J, Glinec Y, Pukhov A, Kiselev S, Gordienko S, Lefebvre E, Rousseau J P, Burgy F and Malka V 2004 *Nature* **431** 541–4

Geddes C G R, Toth C, van Tilborg J, Esarey E, Schoreder C, Bruhwiler D, Nieter C, Cary J and Leemans W 2004 *Nature* **431** 538–41

Hinkel D, Rosen M D, Williams E A, Langdon A B, Still C H, Callahan D A, Moody J D, Michel P A, Town R P J, London R A and Langer S H 2011 *Phys. Plasmas* **18** 056312

Jones T, Krushelnick K, Ting A, Kaganovich D, Moore C and Morozov A 2002 *Rev. Sci. Instrum.* **73** 2259

Kaganovich D, Hafizi B, Palastro J, Ting A, Helle M, Chen Y H, Jones T and Gordon D 2016 *Phys. Plasmas* **23** 123104

Kaganovich D, Ting A C, Helle M H, Gordon D F, Hafizi B and Palastro J 2016 *United States Patent Application Publication* US9370085B2

Kneip S, McGuffey C, Martins J L, Martins S F, Bellei C, Chvykov V, Dollar F, Fonseca R, Huntington C, Kalintchenko G, Maksimchuk A, Mangles S P D, Matsuoka T, Nagel S R, Palmer C A J, Schreiber J, Ta Phuoc K, Thomas A G R, Yanovsky V, Silva L O, Krushelnick K and Najmudin Z 2010 *Nat. Phys.* **6** 980–3

Kono M and Škorić M 2010 *Nonlinear Physics of Plasmas* (*Springer Series on Atomic, Optical, and Plasma Physics* vol 62) (Berlin: Springer) (https://doi.org/10.1007/978-3-642-14694-7)

Krushelnick K, Ting A, Burris H, Fisher A, Manka C and Esarey E 1995 *Phys. Rev. Lett.* **75** 3681

Leemans W, Nagler B, Gonsalves A, Tóth C, Nakamura K, Geddes C, Esarey E, Schroeder C and Hooker S 2006 *Nat. Phys.* **2** 696–9

Lu W, Huang C, Zhou M, Tzoufras M, Tsung F, Mori W and Katsouleas T 2006 *Phys. Plasmas* **13** 056709

Ludwig J, Masson-Laborde P E, Hüller S, Rozmus W and Wilks S 2018 *Phys. Plasmas* **25** 053108

Malka V, Wispelaere E D, Marques J R, Bonadio R, Amiranoff F, Blasco F, Stenz C, Grillon G and Nibbering E 1996 *Phys. Plasmas* **3** 1682

Mangles S P D, Murphy C D, Najmudin Z, Thomas A G R, Collier J L, Dangor A E, Divall E J, Foster P S, Gallacher J G, Hooker C J, Jaroszynski D A, Langley A J, Mori W B, Norreys P A, Tsung F S, Viskup R, Walton B R and Krushelnick K 2004 *Nature* **431** 535–8

Masson-Laborde P, Mo M Z, Ali A, Fourmaux S, Lassonde P, Kieffer J, Rozmus W, Teychenne D and Fedosejevs R 2014 *Phys. Plasmas* **21** 123113

Matsuoka T, McGuffey C, Cummings P G, Horovitz Y, Dollar F, Chvykov V, Kalintchenko G, Rousseau P, Yanovsky V, Bulanov S S, Thomas A G R, Maksimchuk A and Krushelnick K 2010 *Phys. Rev. Lett.* **105** 034801

McGuffey C, Thomas A G R, Schumaker W, Matsuoka T, Chvykov V, Dollar F J, Kalintchenko G, Yanovsky V, Maksimchuk A, Krushelnick K, Bychenkov V Y, Glazyrin I V and Karpeev A V 2010 *Phys. Rev. Lett.* **104** 025004

Miyamoto S, Mima K, Škorić M M and Jovanovic M 1998 *J. Phys. Soc. Jpn.* **67** 1281

Palastro J, Kaganovich D, Gordon D, Hafizi B, Helle M, Penano J and Ting A 2015 *New J. Phys.* **17** 023072

Popov K I, Rozmus W, Bychenkov V Y, Naseri N, Capjack C and Brantov A 2010 *Phys. Rev. Lett.* **105** 195002

Pukhov A and Meyer-ter-Vehn J 2002 *Appl. Phys.* B **74** 355–61

Rousse A, Ta Phuoc K, Shah R, Pukhov A, Lefebvre E, Malka V, Kiselev S, Burgy F, Rousseau J-P, Umstadter D and Hulin D 2004 *Phys. Rev. Lett.* **93** 135005

Shadwick B, Schroeder C and Esarey E 2009 *Phys. Plasmas* **16**

Sprangle P, Esarey E, Krall J and Joyce G 1992 *Phys. Rev. Lett.* **69** 2200

Sprangle P, Esarey E and Ting A 1990 *Phys. Rev. Lett.* **64** 2011

Tajima T and Dawson J M 1979 *Phys. Rev. Lett.* **43** 267

Ting A, Krushelnick K, Burris H R, Fisher A, Manka C and Moore C I 1996 *Opt. Lett.* **21** 1096

Škorić M M, Jovanović M S and Rajković M 1996 *AIP Conf. Proc.* **369** 363

Škorić M, Nikolić L and Ishiguro S 2013 *J. Plasma Phys.* **79** 1003

Walton B, Mangles S P D, Najmudin Z, Tatarakis M, Wei M S, Gopal A, Marle C, Dangor A E, Krushelnick K, Fritzler S, Malka V, Clarke R J and Hernandez-Gomez C 2006 *Phys. Plasmas* **13** 113103

Wang X, Zgadzaj R, Fazel N, Li Z, Yi S A, Zhang X, Henderson W, Chang Y Y, Korzekwa R, Tsai H E, Pai C H, Quevedo H, Dyer G, Gaul E, Martinez M, Bernstein A C, Borger T, Spinks M, Donovan M, Khudik V, Shvets G, Ditmire T and Downer M C 2013 *Nat. Commun.* **4** 1988

Wilks S, Kruer W, Williams E, Amendt P and Eder D 1995 *Phys. Plasmas* **2** 274